

## Article

# Depth Estimation of Sedimentary Sections and Basement Rocks in the Bornu Basin, Northeast Nigeria Using High-Resolution Airborne Magnetic Data

Stephen E. Ekwok<sup>1</sup>, Ogiji-Idaga M. Achadu<sup>2</sup>, Anthony E. Akpan<sup>1</sup>, Ahmed M. Eldosouky<sup>3,\*</sup> ,  
Chika Henrietta Ufuafuonye<sup>1</sup>, Kamal Abdelrahman<sup>4</sup>  and David Gómez-Ortiz<sup>5</sup> 

<sup>1</sup> Applied Geophysics Programme, Department of Physics, University of Calabar, Calabar 540271, Cross River State, Nigeria; styvnekwok@unical.edu.ng (S.E.E.); anthonyakpan@unical.edu.ng (A.E.A.); hufuafuonye@gmail.com (C.H.U.)

<sup>2</sup> Department of Geology, University of Calabar, Calabar 540271, Cross River State, Nigeria; martinsachadu@unical.edu.ng

<sup>3</sup> Department of Geology, Suez University, Suez 43518, Egypt

<sup>4</sup> Department of Geology & Geophysics, College of Science, King Saud University, P.O. Box 2455, Riyadh 11451, Saudi Arabia; khassanein@ksu.edu.sa

<sup>5</sup> Department of Biology and Geology, Physics and Inorganic Chemistry, ESCET, Universidad Rey Juan Carlos, Móstoles, 28933 Madrid, Spain; david.gomez@urjc.es

\* Correspondence: ahmed.eldosouky@sci.suezuni.edu.eg



check for updates

**Citation:** Ekwok, S.E.; Achadu, O.-I.M.; Akpan, A.E.; Eldosouky, A.M.; Ufuafuonye, C.H.; Abdelrahman, K.; Gómez-Ortiz, D. Depth Estimation of Sedimentary Sections and Basement Rocks in the Bornu Basin, Northeast Nigeria Using High-Resolution Airborne Magnetic Data. *Minerals* **2022**, *12*, 285. <https://doi.org/10.3390/min12030285>

Academic Editor: Frank Wendler

Received: 12 January 2022

Accepted: 22 February 2022

Published: 24 February 2022

**Publisher's Note:** MDPI stays neutral with regard to jurisdictional claims in published maps and institutional affiliations.



**Copyright:** © 2022 by the authors. Licensee MDPI, Basel, Switzerland. This article is an open access article distributed under the terms and conditions of the Creative Commons Attribution (CC BY) license (<https://creativecommons.org/licenses/by/4.0/>).

**Abstract:** This study involves the use of high-resolution airborne magnetic data to evaluate the thicknesses of sedimentary series in the Bornu Basin, Northeast Nigeria, using three depth approximation techniques (source parameter imaging, standard Euler deconvolution, and 2D GM-SYS forward modelling methods). Three evenly spaced profiles were drawn in the N-S direction on the total magnetic intensity map perpendicular to the regional magnetic structures. These profiles were used to generate three 2-D models. The magnetic signatures were visually assessed to determine the thickness of depo-centres and the position of intrusions. The thicknesses of sedimentary series based on source parameter imaging results are approximately ranged 286 to 615 m, 695 to 1038 m, and 1145 to 5885 m for thin, intermediate, and thick sedimentation, respectively. Similarly, the standard Euler deconvolution result shows thin (130 to 917 m), intermediate (1044 to 1572 m), and thick (1725 to 5974 m) sedimentation. The magnetic model of Profile 1, characterized by two major breaks, shows that the igneous intrusions and basement rocks are covered by sediments with thickness varying from 300 to <3500 m, while Profile 2 has a maximum estimated depth value of about 5000 m at the southern part. Furthermore, the Profile 3 model shows sediment thicknesses of 2500 and 4500 m in the northern and southern flanks of the profile, respectively. The maximum sediment thickness value from the various depth estimation methods used in this study correlate relatively well with each other. Furthermore, the anomalous depth zone revealed by the 2D forward models coincides with the locality of the thick sedimentation revealed by the source parameter imaging and standard Euler-deconvolution (St-ED) methods. The maximum depth values obtained from the various depth estimation methods used in this study correlated strongly with each other. The widespread occurrence of short-wavelength anomalies in the southern part of the study area as indicated by the jagged nature of the magnetic signature was validated by the analytic signal and upward-continuation results. Generally, it was observed that the southern part of the research area is characterized by thick sedimentation and igneous intrusions.

**Keywords:** aeromagnetic; Bornu Basin; Precambrian; basement depth

## 1. Introduction

Potential field techniques have various successful applications in exploration geophysics [1–10]. One of the most essential applications of the magnetic dataset is to define

the location and depth of magnetic bodies. Conventionally, it is often used to determine sedimentary thicknesses for oil and gas exploration purposes. The false solution problems associated with different depth approximation techniques can be controlled by combining two or more depth determination procedures [11,12], or enhancing the signal/noise ratio through proper evaluation of the derivatives of the field [13].

In this research, vital depth estimation methods like source-parameter imaging (SPI) [14,15], standard-Euler deconvolution (St-ED) [16], and 2D-GM-SYS modelling code [17] in the Oasis–Montaj software (Geosoft Inc., Toronto, ON, Canada) are used for the interpretation of airborne magnetic data collected in the Bornu Basin, Northeast Nigeria. The SPI and St-ED techniques are non-dependent on assumptions about the geologic model [18,19]. Hence, the applications of these techniques have made the procedure of magnetic data interpretation significantly simpler [20]. The use of these depth estimation methods in this study to the same magnetic sources will considerably enhance the reliability of depth solutions. Furthermore, analytic signal [20] and upward-continuation (UP-C) [21–23] filters will be applied to image the location and source of the main tectonics that caused the buried deformations and geologic structures [24,25] within the study area.

Modern geoscience investigations in the Nigerian inland basins are centred on gravity, seismic, magnetic, paleoclimatology, geochemistry, aerial photography, source rocks and rock facies evaluations that have been studied by several researchers [11,26]. At the reconnaissance stage, the basement framework, depositional centres [27], and depth solutions [11,28] can be discerned from high resolution airborne magnetic data. Several researchers [11,23–27,29–33] have investigated the thickness of sediments in the Cretaceous inland basins of Nigeria. In their separate studies, several depth solutions (1.5–12 km) were estimated involving different depth to basement procedures [11]. Remarkably, these investigations have led to the detection of commercial hydrocarbon in the Cretaceous inland Anambra basin. This discovery has further triggered geoscientists' interest to properly evaluate the hydrocarbon prospects of the Nigerian Benue Trough.

Modern airborne (magnetic) data were collected (between 2005 and 2010) by Fugro Airborne-Services, Canada was used in this research. The object of this study which involves the assessment of sediment thicknesses, mapping of basin topography, and delineation of the spatial spread of magnetic sources were resolved using these magnetic datasets. These data can further be employed in the demarcation of regional surficial geologic boundaries [26], mineral assessment programs [11], mapping of hydrothermally modified rocks [27,34–37], edges of sources [38], geothermal potentiality [39], and geologic structures such as faults, fractures, dykes, sills, etc. [27,40]. Furthermore, it can be applied in hydrocarbon exploration [27], archaeological investigations, and unexploded ordnance (UXO) detection [41]. Recently, the readily available high-speed and robust computer programs have made the processes of magnetic data correction, enhancement, modelling, and interpretation easier. Furthermore, the advancements in technology have made it increasingly possible to produce more details, and delineate elusive magnetic anomalies. However, the associated inverse problem of magnetic data is often ill-posed, therefore making the solution unstable and uncertain [42–44]. Nonetheless, a reliable solution to an ill-posed problem can be obtained by combining accurate geologic information with recent innovative magnetic data enhancement and modelling procedures [11].

The Bornu Basin, often described as part of the Upper Benue Trough, is a fraction of the Chad Basin [45]. The basin has witnessed extensive geological and geophysical studies for hydrocarbon, coal and minerals, and groundwater resources [11]. The detection of commercial hydrocarbon in the neighboring Republics of Niger and Chad in the 1970s has further oil and gas exploration activities in the Bornu Basin [46] and other Nigerian inland basins in the last forty years. The geology [45,47,48], stratigraphy [49,50], tectonics and tectono-sedimentary framework of the Nigerian sector of the Chad Basin [24,25,28,51] have been extensively investigated and properly documented. These investigations have indicated a relatively thick succession of sedimentary series overlying coexistent igneous intrusions within the horst/graben structures of the Bornu Basin [23]. The preliminary

results triggered the drilling of twenty-three exploratory wells by the Nigerian National Petroleum Cooperation (NNPC) that revealed evidence of gas accumulation [52].

## 2. Geologic Setting of the Study Area

The investigated region is located at the Northeast Nigeria frontiers with the Republics of Chad, Niger, and Cameroon. It is situated between longitude  $11^{\circ}30'$  E and  $14^{\circ}00'$  E and latitude  $12^{\circ}00'$  N and  $14^{\circ}00'$  N.

The Bornu Basin (Figure 1) is characterized by an elevation ranging from 200–500 m above sea level [15]. It is often described as an interior sag basin [53] and is a portion of the Chad basin [25]. The Chad basin is composed of two coeval rift systems Central African Rift System (CARS) and West African Rift System (WARS) [54] that are physically disconnected but genetically related. The origin of the Central and West African Rift Systems is essentially attributed to the breakup of Gondwana and the opening of the South-Atlantic Ocean and the Indian Ocean at about 120–130 Ma [55].

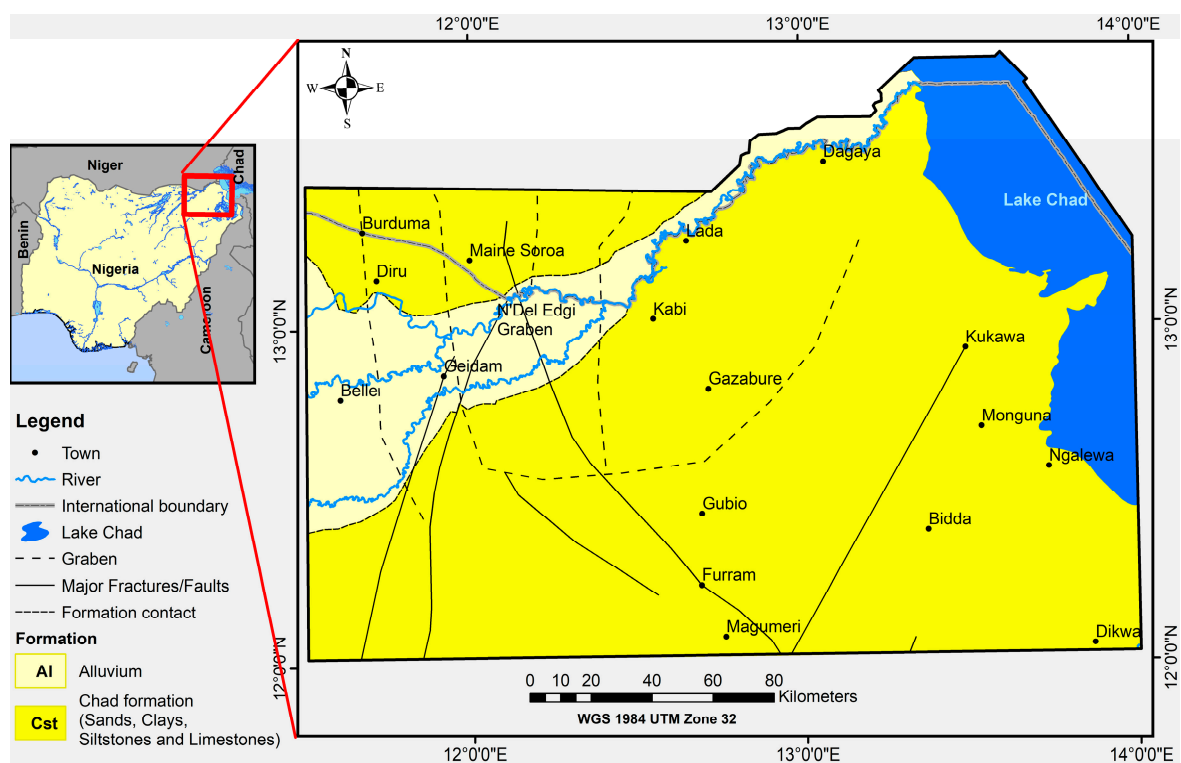


Figure 1. Geologic map of the study area.

The origin and tectonic structure of the Bornu Basin occurred in the evolution period of the WARS [25]. The regional structure and tectonic evolution of the Cretaceous to Recent rift basins of Niger, Chad, and the Central African Republic have been properly studied and well documented [25,55]. Geophysical and geological analyses of data indicate a complex sequence of Cretaceous grabens spanning from the Benue Trough to the southwest [23]. These datasets reveal near-surface intrusive bodies in the horst/graben structures as well as a relatively thick sedimentary section [25].

Refs. [50,56], and others reported the stratigraphic settings of the Southern part of the Chad basin (Figure 2). The Precambrian basement of the basin is directly overlain by continental, sparsely fossiliferous, poorly sorted, and medium to coarse-grained, feldspathic sandstones described as the Bima Formation (Sandstone). Overlying the Bima Formation is the transitional calcareous deposit called Gongila Formation [47,57]. It is composed mainly of sandstone and calcareous shale deposits [23]. This formation shows the beginning of marine incursion into the Chad Basin [58]. Marine transgression in the Albian got to its peak in the Turonian resulting in the deposition of ammonite-rich, bluish-black, open-

marine Fika Shale Formation [58] which continued into Senonian. In the Maastrichtian, the regressive depositional Gombe Sandstone comprised of intercalations of siltstones, ironstones, and shales was deposited in a deltaic/estuarine environment.

| AGE                   | FORMATION             | LITHOLOGY   | THICKNESS (m)    | SEDIMENT THICKNESS FROM SEISMIC DATA (m) | MEAN THICKNESS (m) | DEPOSITIONAL ENVIRONMENT |
|-----------------------|-----------------------|---|------------------|--|--------------------|--------------------------|
| Pliocene, Pleistocene | Chad Formation        | Clay, Sand<br>(Unconformity)                              | Not investigated | 800                                      | 400                | Continental              |
| Palaeocene            | Kerri-Kerri Formation | Coarse Sandstone, Clay stone, Sandstone<br>(Unconformity) | Not investigated |  | 130                | Continental              |
| Maastrichtian         | Gombe Sandstone       | Shale, Sandstone, Siltstone,                              | Not investigated | 0-1000                                   | 315                | Deltaic Estuarine        |
| Turonian-Santonian    | Fika Shale            | Blue-Black Shale  | 840-1453         | 0-900                                    | 430                | Marine                   |
| Turonian              | Gongilla Formation    | Sandstone, Shale  | 162-420          | 0-800                                    | 420                | Marine, Estuarine        |
| Cenomanian            | Bima Formation        | Sandstone<br>(Unconformity)                               | 716-850          | 2000                                     | 3050               | Continental              |
| Crystalline Basement  |                       |   |                  |  |                    |                          |

**Figure 2.** The stratigraphic succession, average thicknesses of formations and thicknesses recorded in the studied wells in the Nigerian sector of the Chad Basin [47,57].

A phase of extensional deformation in the Chad basin occurred between the Late Maastrichtian to the end of the Cretaceous period. This extension deformation created an elongated graben system that trends in the Northeast-Southwest direction. The associated remnant basin that followed this tectonic deformation created a depositional site for the Tertiary Kerri-Kerri Formation that overlies the Cretaceous sedimentary series unconformably [57]. The continental (lacustrine) deposits of the Chad Formation were deposited unconformably over the Kerri-Kerri Formation in the Pleistocene and perhaps, in the Pliocene period. The central and southern parts of the Bornu Basin have witnessed extensive volcanic activity towards the end of the Tertiary, and even recently [59]. Currently, dunes heap up in the Chad basin. The youngest deposits that blanket some parts of the south and southwestern flanks of Lake Chad are the river alluvium and deltaic and lagoonal clay flats [59].

### 3. Materials and Methods

#### 3.1. Data Acquisition

In the middle of 2005 and 2010, Fugro-Airborne Surveys (FAS), Canada, under contract to the Central of Nigeria and supervised by the Nigerian-Geological-Survey Agency (NGSA) collected airborne magnetic data in Nigeria. The data were acquired with Flux-Adjusting Surface Data Assimilation System (FASDAS) with a terrain clearance of between 0.08–0.1 km, tie line spacing of 0.5 km, and flight-line spacing of 0.1 km along 826,000 lines. The flight lines and tie-lines were oriented in the northwest-southeast and northeast-southwest directions, respectively. The tie-lines orientation was carefully and deliberately designed to run across the major geological strike. The 10th generation International Geomagnetic Reference Field (IGRF) version 4.0 was applied by FAS on the compiled dataset to remove IGRF. In magnetic data reduction practice, IGRF, which is easily available and universally accepted, provides consistency in data reduction procedure [60]. Processed

and corrected high-resolution aero-magnetic data are very appropriate for mineral evaluation programs, basin framework, hydrocarbon, and hydrogeological explorations, and delineation of the regional geologic boundary [26,61–67]. The airborne magnetic data employed in this investigation were corrected and processed to a total magnetic intensity map (Figure 3) which were gridded, saved, and displayed in Oasis Montaj Geosoft in colour raster format.

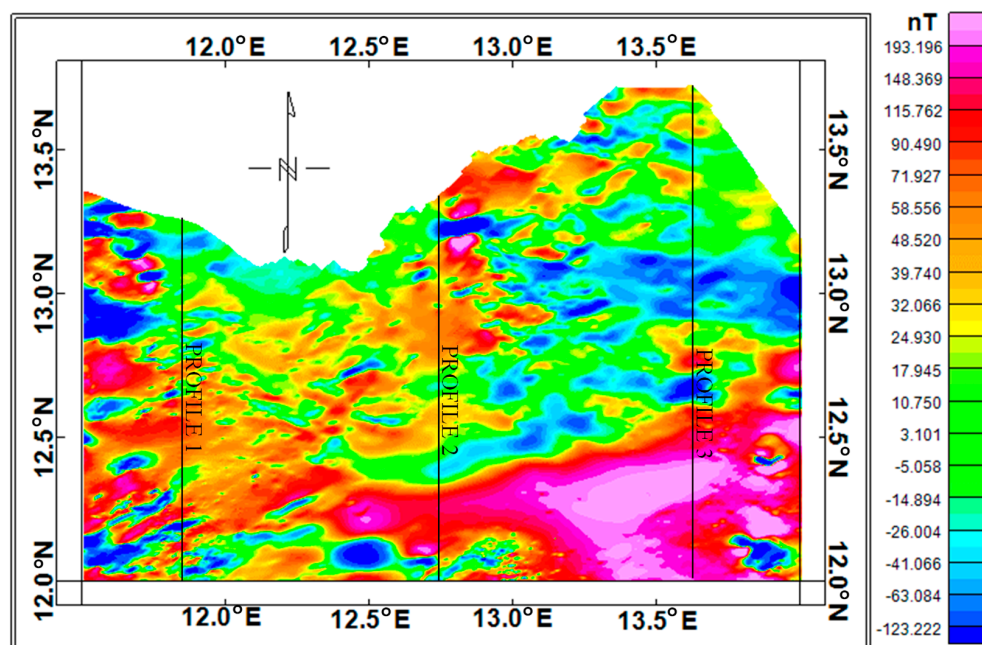


**Figure 3.** Total magnetic intensity map with the profile lines used for modelling.

### 3.2. Data Processing and Modelling

FAS, Canada carried out all the required airborne magnetic data filtering and correction processes. The local datum-transformation and projection method were applied to input magnetic data into World Geodetic System 84 (WGS 84) and Universal Transverse Mercator coordinate system at zone 32 of Northern hemisphere (UTM-32N), respectively. The data file was loaded into source parameter imaging, Euler deconvolution, MAGMAP, and 2-D GM-SYS extensions which generated control files for the various procedures. These processes were comprehensively applied to determine sedimentary thicknesses, define the basement framework, and map the location and the spatial distributions of the main intrusions in the investigated area. The source parameter imaging (SPI) technique [15] output is typically a map from which sediment thicknesses can be estimated [19]. This method evaluates the properties of the second vertical derivative and analytic signal responses [14,19,68]. Just like Euler deconvolution, depth approximation does not depend on any assumptions about the geologic model [19]. Furthermore, the geologic model can be determined correctly from the analysis, and the depth solutions are independent of the magnetic inclination and declination. Consequently, it is not necessary to apply a reduction-to-pole input grid [15]. The magnetic data interpretation procedure is made considerably easier with the availability of correct information on the local geology [15].

The approximations of depth using the SPI method are ordinarily from the wavelength of the analytic signal. Refs. [14,21,69] defined the analytic signal  $A_1(x, z)$  as

$$A_1(x, z) = \frac{\partial M(x, z)}{\partial x} - i \frac{\partial M}{\partial z} \quad (1)$$

where,  $i = \sqrt{-1}$ ,  $M(x, z)$  is the magnitude of the anomalous total magnetic field,  $z$  and  $x$  are the Cartesian coordinates for the vertical and the horizontal directions perpendicular to the strike, respectively.

The standard-Euler deconvolution (St-ED) method relies on Euler's homogeneity equation:

$$(x - x_0) \frac{\partial T}{\partial x} + (y - y_0) \frac{\partial T}{\partial y} + (z - z_0) \frac{\partial T}{\partial z} = N(B - T) \quad (2)$$

where  $(x_0, y_0, z_0)$  is the position of the magnetic field of which total field is observed at  $(x, y, z)$ , while  $B$  is the value of the regional value of the total field. The degree of homogeneity  $N$  is interpreted as a structural index [16]. Unlike several other computer-aided procedures before it, St-ED does not adopt any particular geologic model. In addition, the method which can be applied directly to gridded data is interpreted even when the geology cannot be suitably described by dikes or prisms [69].

Two-dimensional forward modelling [70] involving the GM-SYS tool of Oasis Montaj [42] was used to evaluate depth to the basement and basin framework of the area. The GM-SYS profile is a program for computing magnetic and gravity responses from a cross-section of geologic models [71]. The application of algorithms described by [72] enabled the forward modeling procedure to create a hypothetical geologic model and compute the magnetic/gravity responses based on [73,74]. Generally, the subsurface is partitioned into two layers that are, top sedimentary series and basal basement rock. All points on the profile used for modelling in the GM-SYS platform have values obtained from total magnetic intensity, magnetic susceptibility, geographic coordinates, elevation, inclination, declination, and depth to the basement (generated from source parameter imaging database). The gridded data used for modelling were obtained along with three profiles, drawn mainly in the N-S direction on the total magnetic intensity gridded data (Figure 3). The profile placements were determined after carrying out source parameter imaging and standard Euler operations. These processes were intended to make sure the profile lines were drawn across the depositional centers within the study area. All operations in this investigation were carried out applying codes obtainable in Oasis-Montaj version 7.0.1 (OL) (2008).

The analytic signal (AS) filter ([14,73,74]) generates peak responses over magnetic anomalies. This technique is usually applied at low magnetic latitude because of the in-built problem associated with the reduction-to-pole filter. References [14,20,68] indicated that the amplitude of the AS can be obtained from the three orthogonal derivatives of the magnetic field as:

$$|ASIG_{(x,y)}| = \sqrt{\left(\frac{\partial A}{\partial x}\right)^2 + \left(\frac{\partial A}{\partial y}\right)^2 + \left(\frac{\partial A}{\partial z}\right)^2} \quad (3)$$

where,  $A$  is the observed magnetic field.

Upward-continuation (UP-C) filter is used in evaluating the regional magnetic structures emanating from deeply buried magnetic field sources. The equation of the wavenumber domain filter to generate upward continuation [67] is essential:

$$F(\omega) = e^{-h\omega} \quad (4)$$

where,  $h$  is the continuation height. This function drops progressively with increasing wave-number, decreasing the higher wavenumbers more severely, and so creating a map in which more regional anomalies dominate [60].

#### 4. Results

The SPI and St-ED methods are data enhancement processes for evaluating the positions and depth of magnetic bodies [11]. These methods are suitable for delineating isolated and multiple magnetic source geometries [67], and susceptibility disparity [26]. Wide-ranging colours (pink-blue) showing various depths and locations of different magnetic bodies within the subsurface are displayed by the SPI and St-ED gridded maps (Figure 4). The colour legend bar is described by a negative sign indicating depth measurement from the Earth's surface downward [15]. The SPI (Figure 4a) indicates shallow (red-pink), in-

intermediate (yellow-red) and deep (lemon green-blue) depth ranges of 286 to 615 m, 695 to 1038 m, and 1145 to 5885 m, respectively. Similarly, the standard Euler deconvolution (Figure 4a) reveals the depth to shallow (130 to 917 m), intermediate (1044 to 1572 m), and deep (1725 to 5974 m) magnetic sources characterized by red-pink, yellow-red and lemon green-blue, respectively. The wide range of depth to deep magnetic sources obtained from Figure 4 explains the undulant nature of the underlying basement surface. From the results (Figure 4), zones described by yellow-pink colour (intermediate-high magnetization) are recognized to be localized residual magnetizations associated with ferruginous sediments, horst/graben structures, near-surface igneous intrusions, and related baked sediments of the area [23]. In the late Tertiary, and even in recent times [59], reported extensive volcanic activities in the southern and central parts of the basin. Reference [58] described the area to be blanketed by sand dunes, river alluvium, and deltaic and clay sediments.

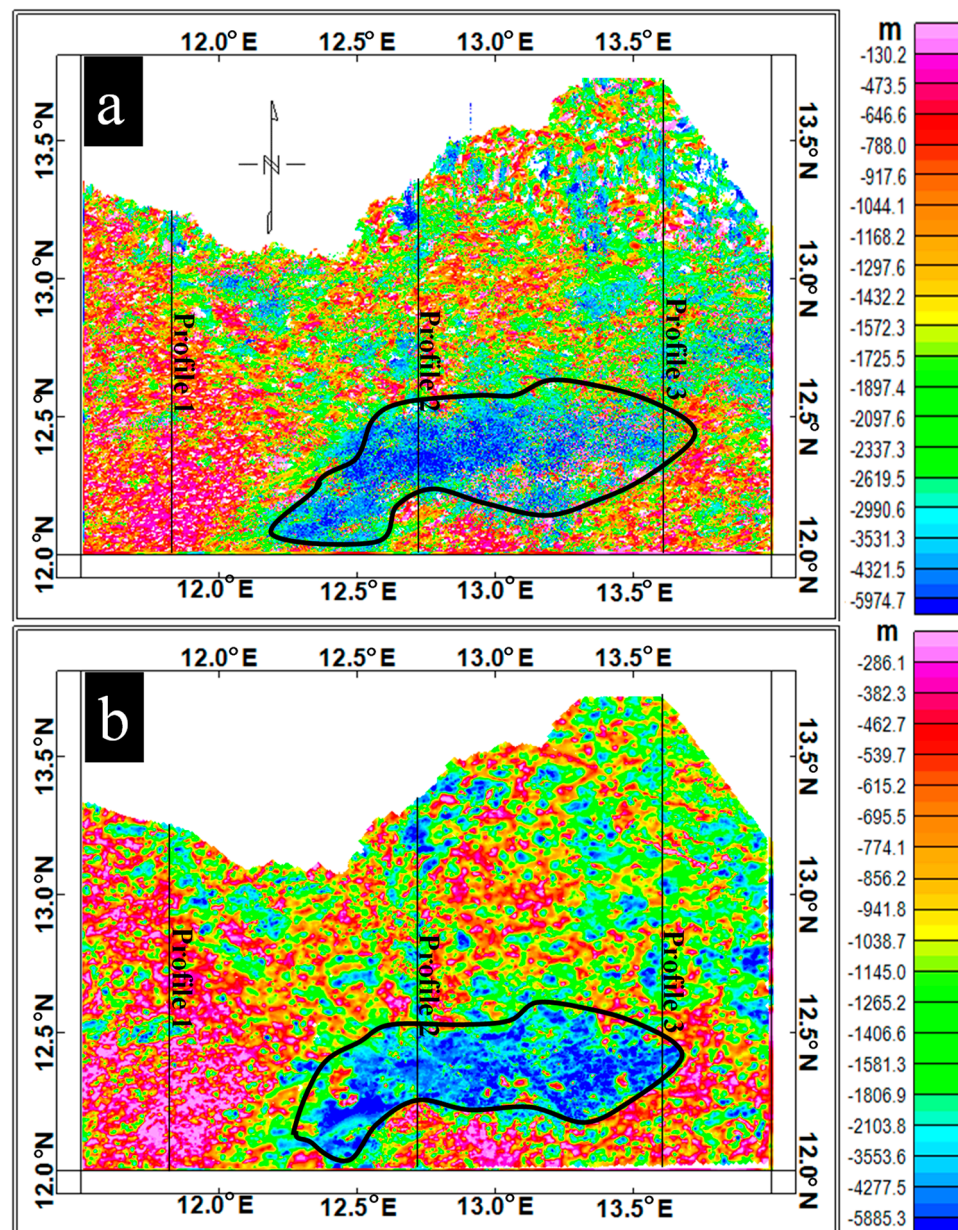
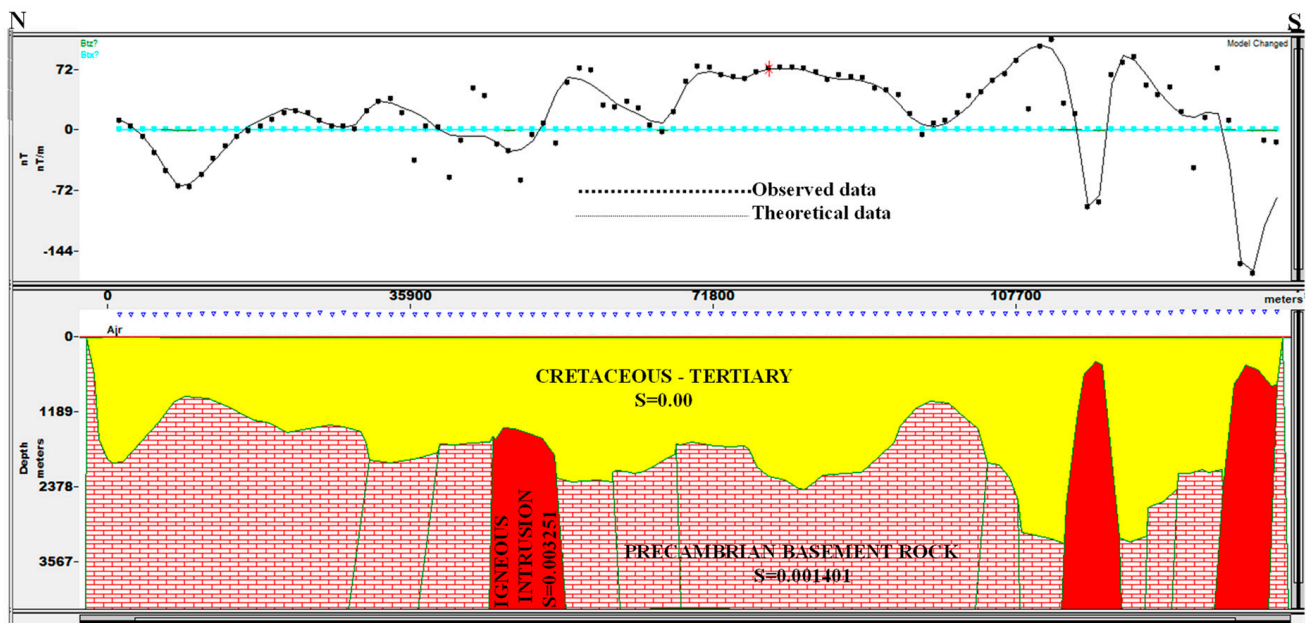


Figure 4. (a) Standard Euler deconvolution (structural index = 1.0; max. % depth tolerance = 15.0, window size = 10) and (b) source parameter imaging maps.

The magnetic signature of Profile 1 (Figure 5), which runs across part of the western flank of the study area in the N-S direction (Figure 3), is characterized by two major breaks around the middle and southern parts of the model. These breaks signify weak zones within the Precambrian basement that created openings for igneous intrusions. These zones of magnetic signature disorders show the occurrence of magnetic anomalies previously revealed by the depth determination techniques (Figure 4). The prevalence of magnetic structures observed along profile 1 indicate the widespread invasion of the Cretaceous-Recent sediments and underlying basement rocks by basaltic lavas, mafic and felsic intrusives [23,25,55,59], whose sizes range from dyke-like structures to massive granitic structures that may perhaps link to generate massive structures [11,28]. In general, Profile 1 model shows that the igneous intrusions and basement rocks are blanketed by sedimentary series with thickness varying from ~300 to <3500 m.



**Figure 5.** 2-D total magnetic intensity model obtained at Profile 1 showing thickness of sediments, basement and igneous rocks, and their respective susceptibility values.

Furthermore, the model obtained at the centre that runs in the N-S direction (Profile 2, Figure 6) is defined by having one serration towards the northern part of the magnetic signature. This is an indication of magnetic intrusion that penetrated the weak zone within the basement and overlying sediments. The southern end of the model is characterized by an anomalous depth [25] value of about 5000 m. This region coincides with the thick sediments zone previously circumscribed by a black polygon in Figure 4.

Profile 3 is situated at the eastern flank runs in the N-S direction (Figure 3). It is characterized by jagged and smooth magnetic signature at the southern and northern ends, respectively (Figure 7). The serrated pattern of the curve at the southern part shows multiple block faults within the basement and overlying sediments caused by tectonic events [25,49,55]. In general, the model shows sediments cover of about 2500 and 4500 m in the northern and southern flanks of the profile, respectively. The region with thick sediments falls under the southern flank of the model. This anomalous depth region that runs east-west coincides with the locality of the thick sedimentation revealed by Figures 4 and 6.

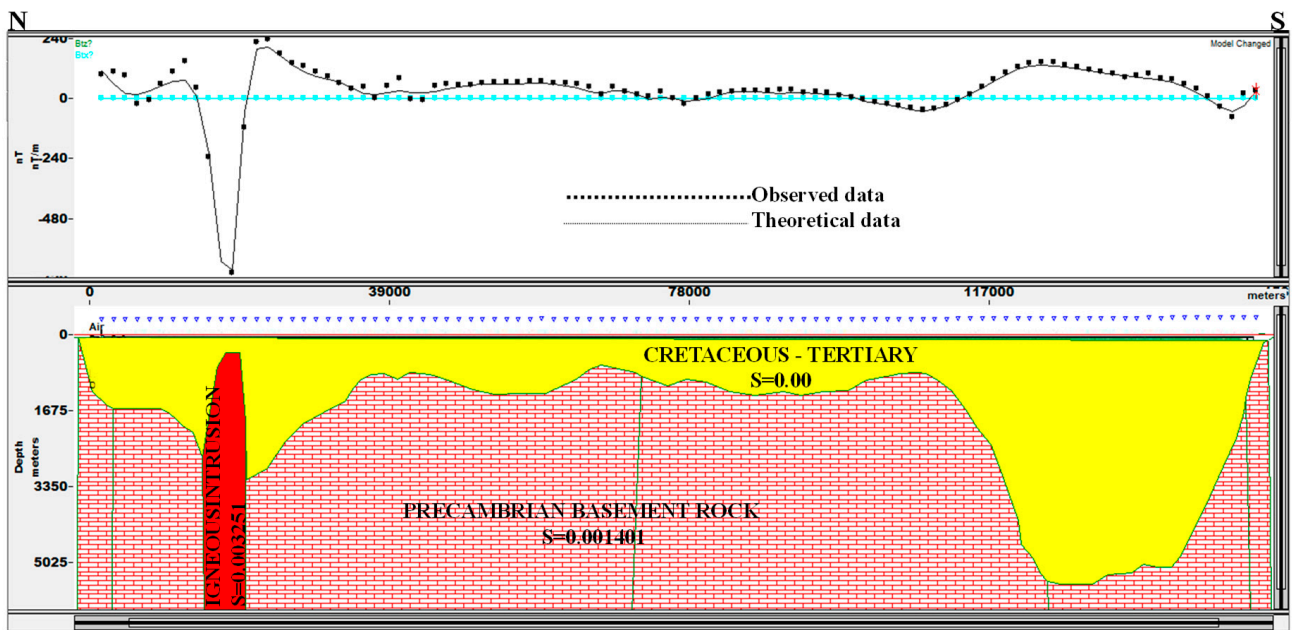


Figure 6. 2-D total magnetic intensity model obtained at Profile 2 showing thickness of sediments, basement and igneous rocks, and their respective susceptibility values.

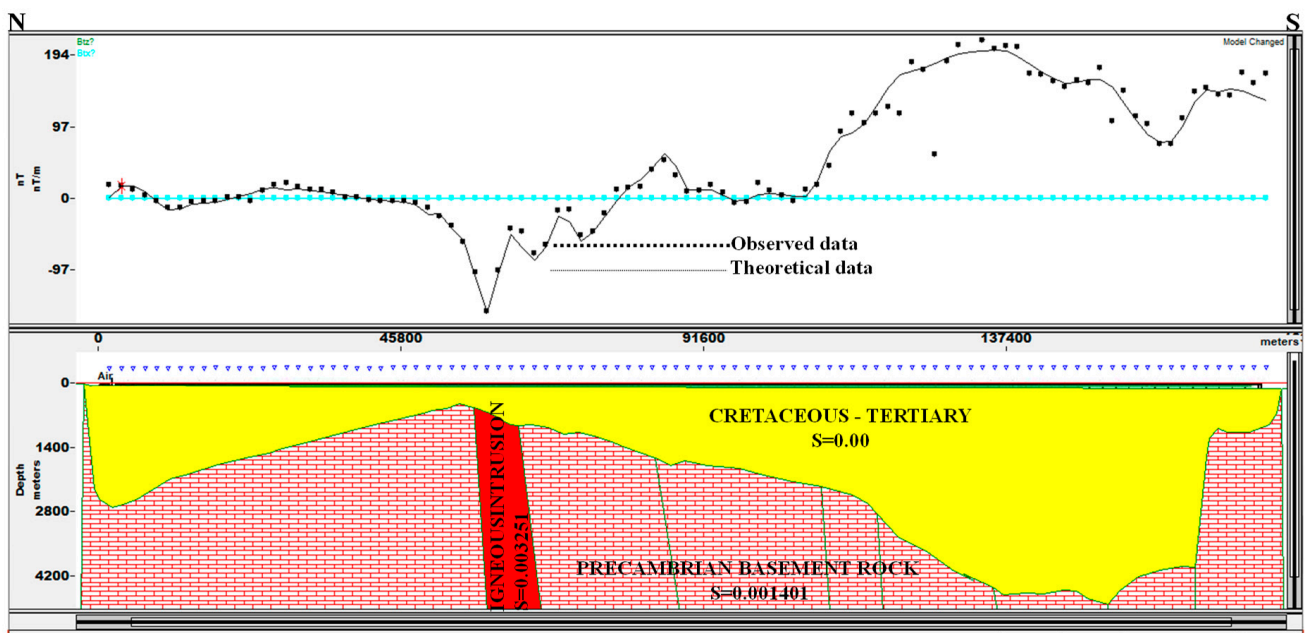


Figure 7. 2-D total magnetic intensity model obtained at Profile 3 showing thickness of sediments, basement and igneous rocks, and their respective susceptibility values.

Analytic signal (AS) filter [21] creates peak responses over distinctive magnetic bodies. The amplitude of magnetization mostly generated by the AS is independent of the direction of the magnetic body [21]. Figure 8a outlined low (0.003421–0.008461 nT/m), intermediate (0.009898–0.017579 nT/m) and high (0.019647–0.093958 nT/m) magnetizations described by blue, lemon green-yellow and red-pink colours correspondingly. The delineated regions of high magnetizations (red-pink colours) labeled A, B and C correlate with the sites of near-surface igneous intrusions (Figure 8a) occurring alongside the horst/graben structures in the Bornu Basin described by [23,25]. Similarly, Figure 8a delineated the U-like structure dominated by low-intermediate magnetizations (blue-yellow colours).

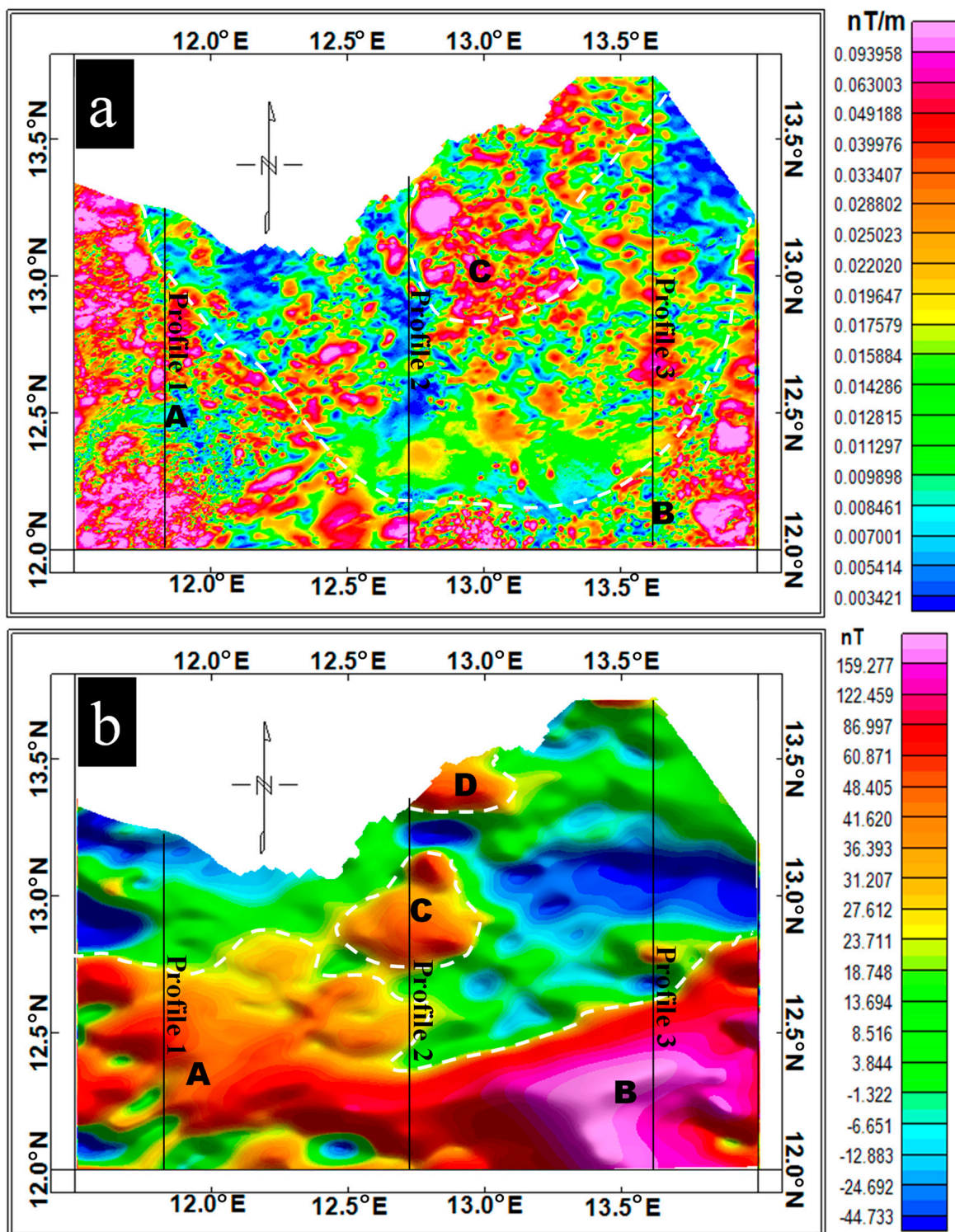


Figure 8. (a) Analytic signal and (b) total magnetic intensity data upward continued 5000 m maps.

To reveal the main igneous intrusions that caused near-surface magnetizations, geologic structures, baking of basement and overlying sedimentary materials, the upward continuation filter [20,75] was applied to the magnetic data. The data were upward continued to 5000 m (Figure 8b) to eliminate magnetic effects emanating from high-frequency magnetic bodies. Figure 8b displays a deeply seated ridge-like intrusive structure (labeled as A-B dominated by red-pink colours) that straddles the southern part of the study area in the E-W direction. Furthermore, Figure 8b showed igneous intrusions in the central and

the northern parts of the investigated area labeled as C and D, respectively. The location of these igneous validates the findings of [59]. Furthermore, A, B, C, and D igneous intrusions match with the anticlinal structures of the study area that are sandwiched by synclines (well-defined by lemon green-blue colours). Additionally, Figure 8b showed a distinct deeply buried E-W weak zone well defined by blue colour at the eastern flank of the area. Similar features observed at the northwestern flank correlate with the location of N'Dgel Edgi graben that extends into Nigeria from the Niger Republic [24]. These regions characterized by intermediate magnetizations (Figure 8a) are dominated by intermediate-thick sedimentations (Figure 4).

## 5. Discussion

The Bornu Basin, which is part of the Upper Benue Trough [45], is described by [53] as an interior sag basin that is genetically interrelated to the Central African Rift System and West African Rift System [54]. The area is characterized by sedimentary thicknesses in the range of about 130 to 5974 m from SPI, St-ED, and 2-D modeling results (Figures 4–7). The respective peak depth values of 5885 m, 5974 m, and 5500 m revealed from the various depth determination methods used, strongly agree with each other. The depth results match relatively well with the depth estimation results obtained by previous researchers in the Bornu Basin [25,30,32,33,49]. Similarly, studies carried out in the genetically and structurally connected Lower Benue Trough, involving potential field data and various depth estimation methods [11,26,27,31,34,59,76] show strong correlation with depth solutions of the Bornu Basin. However, [29,47] reported contrary sedimentary thicknesses of about 10,000 m and 9000 m, in the Bornu Basin and Lower Benue Trough, respectively.

Additionally, an anomalous sedimentary thickness (Figure 4) represented by a polygon sits on igneous intrusions revealed by the UP-C magnetic map (Figure 8b). Documented geophysical and geological works revealed that the investigated area is dominated by horst/graben structures, block faults, and associated igneous intrusions [24,25,55]. However, the findings of [23] and others indicated that these structures are blanketed by somewhat thick sediments. Their reports motivated the Nigerian National Petroleum Corporation (NNPC) to drill some exploratory wells within the area characterized by thick sedimentation. The exploration exercise revealed evidence of gas accumulation [52] which may perhaps be caused by igneous intrusions [56,58] and related enhanced geothermal gradient. The 2-D models with sediment thicknesses in the range of ~300 to ~5500 m (Figures 5–7) obtained from the three profiles (Figure 3) are characterized by jagged magnetic signatures. The serrated pattern of the curves indicates multiple block faults within the basement, and widespread invasion of igneous intrusions into overlying Cretaceous sediments [23,25,55,59]. These igneous invasions were detected by SPI and St-ED (Figure 4), as well as analytic signal and upward continuation enhancements (Figure 8). Geologic structures caused by intrusions in such regions are the potential pathway for hydrothermal fluid migration and mineralization in rift environments [18,34,64,77–79] like the Bornu Basin. However, Figure 8b revealed E-W anticlinal structures (red-pink colour) adjoined by a trough-like structure (lemon green-blue colour) located at the southern and northern parts of the study area, respectively. The northern part is characterized by two isolated domal high magnetization structures and E-W weak zone (blue colour) separating them. The western end of this weak zone runs into N'Dgel Edgi graben, Niger Republic [25], where commercial hydrocarbon is exploited. Generally, the northern flank of the study area is characterized by intermediate depths (Figure 5) and magnetizations (Figure 8). Hence, further oil and gas surveys involving drilling of exploratory wells and seismic reflection techniques should be shifted to this area defined by insignificant relics of post-Cretaceous tectonic events [26].

## 6. Conclusions

Modern high-resolution aero-magnetic data measured between 2005 and 2010 were used to infer thicknesses of the sedimentary sections of Northeastern Nigeria. Various

depth estimation methods like source parameter imaging (SPI), Standard-Euler deconvolution (St-ED), and 2D GM-SYS forward modelling were used in this investigation. It was generally observed from the various results obtained that the southern part of the study area is dominated by thick sedimentary series coexistent with igneous intrusions. The SPI result revealed 286 to 615 m, 695 to 1038 m, and 1145 to 5885 m for thin, intermediate, and thick sedimentation, respectively. Likewise, the St-ED result indicated values of 130 to 917 m, 1044 to 1572 m, and 1725 to 5974 m for thin, intermediate, and thick sedimentation correspondingly. A 2D forward model of Profile 1 is described by two major breaks, indicating that the igneous intrusions and basement rocks are blanketed by sediments with thicknesses ranging from about 300 to <3500 m while the 2D model of Profile 2 has an approximated maximum depth value of about 5000 m at the southern flank. Furthermore, the Profile 3 model shows sedimentary thickness in the range of 2500 and 4500 m in the northern and southern ends of the profile, respectively. The anomalous depth region detected by the 2D forward models matches with the location of the thick sedimentary cover identified by the SPI and St-ED techniques. The maximum depth values obtained from the different depth approximation procedures employed in this investigation matched closely with each other. In addition, the forward models revealed that the underlying basement framework is undulant, and the weak zones intruded by igneous rocks. Further hydrocarbon investigations involving the seismic reflection method and exploratory wells should be shifted to the northern flank characterized by shallow-intermediate depths and magnetizations. On the whole, the extensive occurrence of igneous intrusions in the southern part of the study area have caused severe fracturing and faulting of the basement, and overlying sediments. Related geologic structures caused by tectonic events serve as a potential pathway for hydrothermal fluid migration and mineralization accumulation. High resolution ground gravity and electromagnetic studies should be employed in the exploration of igneous rock related minerals.

**Author Contributions:** Conceptualization, S.E.E. and O.-I.M.A.; methodology, O.-I.M.A.; software, S.E.E.; validation, A.E.A., S.E.E. and C.H.U.; formal analysis, C.H.U.; investigation, A.E.A.; resources, S.E.E.; data curation, C.H.U.; writing—original draft preparation, S.E.E., O.-I.M.A. and A.M.E.; writing—review and editing, S.E.E., O.-I.M.A. and A.M.E.; visualization, S.E.E., O.-I.M.A. and A.M.E.; supervision, S.E.E., A.E.A., D.G.-O. and A.M.E.; project administration, S.E.E.; funding acquisition, K.A. All authors have read and agreed to the published version of the manuscript.

**Funding:** This research was funded by [King Saud University, Riyadh, Saudi Arabia] grant number [RSP-2022/351] And The APC was funded by [Researchers Supporting Project number (RSP-2022/351), King Saud University, Riyadh, Saudi Arabia].

**Data Availability Statement:** Data available on request from the authors.

**Acknowledgments:** Deep thanks and gratitude to the Researchers Supporting Project number (RSP-2022/351), King Saud University, Riyadh, Saudi Arabia for funding this research article.

**Conflicts of Interest:** There are no potential conflict exist in the paper. There is no declaration of interest.

## References

1. Koné, A.Y.; Nasr, I.H.; Traoré, B.; Amiri, A.; Inoubli, M.H.; Sangaré, S.; Qaysi, S. Geophysical Contributions to Gold Exploration in Western Mali According to Airborne Electromagnetic Data Interpretations. *Minerals* **2021**, *11*, 126. [[CrossRef](#)]
2. Fu, J.; Jia, S.; Wang, E. Combined Magnetic, Transient Electromagnetic, and Magnetotelluric Methods to Detect a BIF-Type Concealed Iron Ore Body: A Case Study in Gongchangling Iron Ore Concentration Area, Southern Liaoning Province, China. *Minerals* **2020**, *10*, 1044. [[CrossRef](#)]
3. Mehane, S.; Zhdanov, M. A quasi-analytical boundary condition for three-dimensional finite difference electromagnetic modeling. *Radio Sci.* **2004**, *39*, RS6014. [[CrossRef](#)]
4. Mehane, S.; Golubev, N.; Zhdanov, M.S. Weighted regularized inversion of magnetotelluric data. In *SEG Technical Program Expanded Abstracts 1998*; Society of Exploration Geophysicists: Tulsa, OK, USA, 1998; pp. 481–484. [[CrossRef](#)]

5. Biswas, A.; Mandal, A.; Sharma, S.P.; Mohanty, W.K. Delineation of subsurface structures using self-potential, gravity, and resistivity surveys from South Purulia Shear Zone, India: Implication to uranium mineralization. *Interpretation* **2014**, *2*, T103–T110. [[CrossRef](#)]
6. Biswas, A.; Rao, K. Interpretation of Magnetic Anomalies over 2D Fault and Sheet-Type Mineralized Structures Using Very Fast Simulated Annealing Global Optimization: An Understanding of Uncertainty and Geological Implications. *Lithosphere* **2021**, *2021*, 2964057. [[CrossRef](#)]
7. Essa, K.S.; Mehane, S.; Elhoussein, M. Magnetic Data Profiles Interpretation for Mineralized Buried Structures Identification Applying the Variance Analysis Method. *Pure Appl. Geophys.* **2020**, *178*, 973–993. [[CrossRef](#)]
8. Gan, J.; Li, H.; He, Z.; Gan, Y.; Mu, J.; Liu, H.; Wang, L. Application and Significance of Geological, Geochemical, and Geophysical Methods in the Nanpo Gold Field in Laos. *Minerals* **2022**, *12*, 96. [[CrossRef](#)]
9. Liu, Y.; Na, X.; Yin, C.; Su, Y.; Sun, S.; Zhang, B.; Ren, X.; Baranwal, V.C. 3D joint inversion of airborne electromagnetic and magnetic data based on local Pearson correlation constraints. *IEEE Trans. Geosci. Remote Sens.* **2022**. [[CrossRef](#)]
10. Mehane, S.A. A new scheme for gravity data interpretation by a faulted 2-D horizontal thin block: Theory, numerical examples and real data investigation. *IEEE Trans. Geosci. Remote Sens.* **2022**. [[CrossRef](#)]
11. Ekwok, S.E.; Akpan, A.E.; Ebong, E.D.; Eze, O.E. Assessment of depth to magnetic sources using high resolution aero-magnetic data of some parts of the Lower Benue Trough and adjoining areas, Southeast Nigeria. *Adv. Space Res.* **2021**, *67*, 2104–2119. [[CrossRef](#)]
12. Salem, A.; Ravat, D. A combined analytic signal and Euler method (AN-EUL) for automatic interpretation of magnetic data. *Geophysics* **2003**, *68*, 1952–1961. [[CrossRef](#)]
13. Davis, K.; Li, Y. Enhancement of depth estimation techniques with amplitude analysis. In *SEG Technical Program Expanded Abstracts 2009*; Society of Exploration Geophysicists: Tulsa, OK, USA, 2009; pp. 908–912. [[CrossRef](#)]
14. Mehane, S.; Essa, K.S.; Diab, Z.E. Magnetic Data Interpretation Using a New R-Parameter Imaging Method with Application to Mineral Exploration. *Nonrenew. Resour.* **2020**, *30*, 77–95. [[CrossRef](#)]
15. Thurston, J.B.; Smith, R.S. Automatic conversion of magnetic data to depth, dip, and susceptibility contrast using SPITM method. *Geophysics* **1997**, *62*, 807–813. [[CrossRef](#)]
16. Reid, A.B.; Allsop, J.M.; Granser, H.; Millett, A.J.; Somerton, I.W. Magnetic interpretation in three dimensions using Euler deconvolution. *Geophysics* **1990**, *55*, 80–91. [[CrossRef](#)]
17. Northwest Geophysical Associates (NGA), Inc. GM-SYS Gravity/Magnetic Modeling Software, User’s Guide, Version 4.9. 2004. pp. 1–101. Available online: [http://pages.geo.wvu.edu/~wilson/gmsys\\_49.pdf](http://pages.geo.wvu.edu/~wilson/gmsys_49.pdf) (accessed on 9 January 2022).
18. Elkhateeb, S.O.; Eldosouky, A.M. Detection of porphyry intrusions using analytic signal (AS), Euler Deconvolution, and Centre for Exploration Targeting (CET) Technique Porphyry Analysis at Wadi Allaqi Area, South Eastern Desert, Egypt. *Int. J. Eng. Res.* **2016**, *7*, 471–477.
19. Smith, R.S.; Thurston, J.B.; Dai, T.; MacLeod, I.N. ISPITM—The improved source parameter imaging method. *Geophys. Prospect.* **1998**, *46*, 141–151. [[CrossRef](#)]
20. Roest, W.; Verhoef, J.; Pilkington, M. Magnetic interpretation using the 3-D analytic signal. *Geophysics* **1992**, *57*, 116–125. [[CrossRef](#)]
21. Nabighian, M.N. The analytical signal of two dimensional magnetic bodies with polygon cross-section: Its properties and use for automated anomaly interpretation. *Geophysics* **1972**, *37*, 507–517. [[CrossRef](#)]
22. Nabighian, M.N. Towards the three-dimensional automatic interpretation of potential field data via generalized Hilbert transforms. Fundamental relations. *Geophysics* **1984**, *53*, 957–966. [[CrossRef](#)]
23. Nwankwo, C.N.; Emujakporue, G.O.; Nwosu, L.I. Evaluation of the petroleum potentials and prospect of the Chad Basin Nigeria from heat flow and gravity data. *J. Pet. Explor. Prod. Technol.* **2011**, *2*, 1–6. [[CrossRef](#)]
24. Genik, G.J. Regional framework structure and petroleum aspects of the rift basins in Niger, Chad and Central African Republic (C.A.R.). *Tectonophysics* **1992**, *213*, 169–185. [[CrossRef](#)]
25. Genik, G.J. Petroleum geology of Cretaceous to Tertiary rift basins in Niger, Chad and the Central African Republic. *Bull. Am. Assoc. Pet. Geol.* **1993**, *77*, 1405–1434.
26. Ekwok, S.E.; Akpan, A.E.; Ebong, D.E. Enhancement and modelling of aeromagnetic data of some inland basins, southeastern Nigeria. *J. Afr. Earth Sci.* **2019**, *155*, 43–53. [[CrossRef](#)]
27. Ekwok, S.E.; Akpan, A.E.; Ebong, E.D. Assessment of crustal structures by gravity and magnetic methods in the Calabar Flank and adjoining areas of Southeastern Nigeria—A case study. *Arab. J. Geosci.* **2021**, *14*, 308. [[CrossRef](#)]
28. Ofoegbu, C.O. A model for the tectonic evolution of the Benue Trough of Nigeria. *Geol. Rundsch.* **1984**, *73*, 1007–1018. [[CrossRef](#)]
29. Abdullahi, M.; Kumar, R.; Singh, U.K. Magnetic basement depth from high-resolution aeromagnetic data of parts of lower and middle Benue Trough (Nigeria) using scaling spectral method. *J. Afr. Earth Sci.* **2018**, *150*, 337–345. [[CrossRef](#)]
30. Ola, P.S.; Adekoya, J.A.; Olabode, S.O. Source Rock Evaluation in the Lake Chad area of the Bornu Basin, Nigeria. *J. Pet. Environ. Biotechnol.* **2017**, *8*, 346.
31. Oha, I.A.; Onuoha, K.M.; Nwegbu, A.N.; Abba, A.U. Interpretation of high resolution aeromagnetic data over southern Benue Trough, southeastern Nigeria. *J. Earth Syst. Sci.* **2016**, *125*, 369–385. [[CrossRef](#)]
32. Olabode, S.O.; Adekoya, J.A.; Ola, P.S. Distribution of sedimentary formations in the Bornu Basin, Nigeria. *Pet. Explor. Dev.* **2015**, *42*, 674–682. [[CrossRef](#)]

33. Umar, T. Geologie Petroliere du Secteur Nigerian du Basin du Lac Tchad. Unpublished Ph.D. Dissertation, Universite de Pau et des Pays de l'Adour, Centre Universitaire de Recherche Scientifique Laboratoire de Geodynamique et Modelisation des Bassins Sedimentaires, Pau, France, 1999; 425p. Available online: <https://www.theses.fr/1999PAUU3013> (accessed on 9 January 2022).
34. Ekwok, S.E.; Akpan, A.E.; Kudamnya, E.A. Exploratory mapping of structures controlling mineralization in South-east Nigeria using high resolution airborne magnetic data. *J. Afr. Earth Sci.* **2020**, *162*, 103700. [[CrossRef](#)]
35. Eldosouky, A.; Sehsah, H.; Elkhateeb, S.O.; Pour, A.B. Integrating aeromagnetic data and Landsat-8 imagery for detection of post-accretionary shear zones controlling hydrothermal alterations: The Allaqi-Heiani Suture zone, South Eastern Desert, Egypt. *Adv. Space Res.* **2019**, *65*, 1008–1024. [[CrossRef](#)]
36. Eldosouky, A.M.; Mohamed, H. Edge detection of aeromagnetic data as effective tools for structural imaging at Shilman area, South Eastern Desert, Egypt. *Arab. J. Geosci.* **2021**, *14*, 13. [[CrossRef](#)]
37. Elkhateeb, S.O.; Eldosouky, A.M.; Khalifa, M.O.; Aboalhassan, M. Probability of mineral occurrence in the Southeast of Aswan area, Egypt, from the analysis of aeromagnetic data. *Arab. J. Geosci.* **2021**, *14*, 1514. [[CrossRef](#)]
38. Eldosouky, A.M.; El-Qassas, R.A.; Pour, A.B.; Mohamed, H.; Sekandari, M. Integration of ASTER satellite imagery and 3D inversion of aeromagnetic data for deep mineral exploration. *Adv. Space Res.* **2021**, *68*, 3641–3662. [[CrossRef](#)]
39. Melouah, O.; Eldosouky, A.M.; Ebong, E.D. Crustal architecture, heat transfer modes and geothermal energy potentials of the Algerian Triassic provinces. *Geothermics* **2021**, *96*, 102211. [[CrossRef](#)]
40. Eldosouky, A.M.; Elkhateeb, S.O. Texture analysis of aeromagnetic data for enhancing geologic features using co-occurrence matrices in Elallaqi area, South Eastern Desert of Egypt. *NRIAG J. Astron. Geophys.* **2018**, *7*, 155–161. [[CrossRef](#)]
41. Essa, K.S.; Elhussein, M. PSO (particle swarm optimization) for interpretation of magnetic anomalies caused by simple geometrical structures. *Pure Appl. Geophys.* **2018**, *175*, 3539–3553. [[CrossRef](#)]
42. Pallero, J.L.G.; Fernández-Martínez, J.L.; Bonvalot, S.; Fudym, O. Gravity inversion and uncertainty assessment of basement relief via Particle Swarm Optimization. *J. Appl. Geophys.* **2015**, *116*, 180–191. [[CrossRef](#)]
43. Ekinci, Y.L.; Balkaya, Ç.; Göktürkler, G.; Özyalın, Ş. Gravity data inversion for the basement relief delineation through global optimization: A case study from the Aegean Graben System, western Anatolia, Turkey. *Geophys. J. Int.* **2020**, *224*, 923–944. [[CrossRef](#)]
44. Essa, K.S.; Elhussein, M. A new approach for the interpretation of magnetic data by a 2-D dipping dike. *J. Appl. Geophys.* **2017**, *136*, 431–443. [[CrossRef](#)]
45. Okosun, E.A. Review of the geology of Bornu Basin. *J. Min. Geol.* **1995**, *31*, 113–122.
46. Nwazeapu, A.U. Hydrocarbon Exploration in Frontier Basin: The Nigeria Chad Basin Experience. In Proceedings of the 28th Annual Conference of the Nigerian Mining and Geosciences Society, Port Harcourt, Nigeria, 1–5 March 1992.
47. Avbovbo, A.A.; Ayoola, E.O.; Osahon, G.A. Depositional and structural styles in Chad Basin of north-eastern Nigeria. *AAPG Bull.* **1986**, *70*, 1787–1798.
48. Okosun, E. Cretaceous ostracod biostratigraphy from Chad Basin in Nigeria. *J. Afr. Earth Sci.* **1992**, *14*, 327–339. [[CrossRef](#)]
49. Nwankwo, C.N.; Ekine, A.S. Geothermal Gradients in the Chad Basin, Nigeria, from bottom hole temperature logs. *Int. J. Phys. Sci.* **2009**, *4*, 777–783.
50. Okosun, E.A. A preliminary assessment of the petroleum potentials from southwest Chad Basin (Nigeria). *Borno J. Geol.* **2000**, *2*, 40–50.
51. Nwachukwu, S.O. The tectonic evolution of the the southern portion of the Benue Trough, Nigeria. *Geol. Mag.* **1972**, *109*, 411–419. [[CrossRef](#)]
52. Moumouni, A.; Obaje, N.G.; Nzegbuna, A.I.; Chanda, M.S. Bulk geochemical parameters and biomarker characteristics of organic matter in two wells (Gaibu-1 and Kasade-1) from Bornu Basin: Implications on hydrocarbon potentials. *J. Pet. Geosci. Eng.* **2007**, *58*, 275–282. [[CrossRef](#)]
53. Kingston, D.R.; Dishroon, C.P.; Williams, P.A. Hydrocarbon plays and global basin classification. *AAPG Bull.* **1983**, *67*, 2194–2197.
54. Hamza, H.; Hamidu, I. Hydrocarbon resource potential of the Bornu Basin Northeastern Nigerian. *Glob. J. Geol. Sci.* **2011**, *10*, 71–84.
55. Fairhead, J.; Green, C. Controls on rifting in Africa and the regional tectonic model for the Nigeria and East Niger rift basins. *J. Afr. Earth Sci.* **1989**, *8*, 231–249. [[CrossRef](#)]
56. Petters, S.W.; Ekweozor, C.M. Petroleum geology of Benue Trough and southeastern Chad Basin Nigeria. *AAPG Bull.* **1982**, *66*, 1141–1149.
57. Carter, J.D.; Barber, W.; Jones, G.P. The geology of parts of Adamawa, Bauchi and Bornu provinces in north-eastern Nigeria. *Bull. Geol. Sum. Nigeria* **1963**, *30*, 109.
58. Olugbemi, R.O.; Ligouis, B.; Abaa, S.I. The Cretaceous series in the Chad Basin, NE Nigeria source rock potential and thermal maturity. *J. Pet. Geol.* **1997**, *20*, 51–58. [[CrossRef](#)]
59. Burke, K. The chad basin: An active intra-continental basin. *Tectonophysics* **1976**, *36*, 197–206. [[CrossRef](#)]
60. Reeves, C.; Reford, S.; Millingan, P. Airborne Geophysics: Old Methods, New Images. In *Proceedings of the Fourth Decennial International Conference on Mineral Exploration*; Prospectors and Developers Association: Toronto, ON, Canada, 1997; pp. 13–30. Available online: <https://www.worldcat.org/title/geophysics-and-geochemistry-at-the-millennium-proceedings-of-exploration-97-fourth-decennial-international-conference-on-mineral-exploration/oclc/40988105> (accessed on 9 January 2022).
61. United States Geological Survey (USGS). Setting and Origin of Iron Oxide Copper-Cobalt-Gold-Rare Earth Element Deposits of Southeast Missouri. 2013. Available online: <http://minerals.usgs.gov/east/semissouri/index.html> (accessed on 9 January 2022).

62. Eldosouky, A.M.; Abdelkareem, M.; Elkhateeb, S.O. Integration of remote sensing and aeromagnetic data for map-ping structural features and hydrothermal alteration zones in Wadi Allaqi area, South Eastern Desert of Egypt. *J. Afr. Earth Sci.* **2017**, *130*, 28–37. [[CrossRef](#)]
63. Shebl, A.; Abdellatif, M.; Elkhateeb, S.; Csámer, Á. Multisource Data Analysis for Gold Potentiality Mapping of Atalla Area and Its Environs, Central Eastern Desert, Egypt. *Minerals* **2021**, *11*, 641. [[CrossRef](#)]
64. Ekwok, S.E.; Akpan, A.E.; Achadu, O.-I.M.; Eze, O.E. Structural and lithological interpretation of aero-geophysical data in parts of the Lower Benue Trough and Obudu Plateau, southeast Nigeria. *Adv. Space Res.* **2021**, *68*, 2841–2854. [[CrossRef](#)]
65. Ekwok, S.E.; Akpan, A.E.; Kudamnya, E.A.; Ebong, D.E. Assessment of groundwater potential using geophysical data: A case study in parts of Cross River State, south-eastern Nigeria. *Appl. Water Sci.* **2020**, *10*, 144. [[CrossRef](#)]
66. Kearey, P.; Brooks, M.; Hill, I. *An Introduction to Geophysical Exploration*, 3rd ed.; Blackwell Science Ltd. Editorial Offices: New York, NY, USA, 2002.
67. Telford, W.M.; Geldart, L.P.; Sheriff, R.E. *Applied Geophysics*, 2nd ed.; Cambridge University Press: Cambridge, UK, 1990.
68. Casto, D.W. *Calculating Depths to Shallow Magnetic Sources Using Aeromagnetic Data from the Tucson Basin*; US Department of the Interior: Washington, DC, USA, 2001. [[CrossRef](#)]
69. Essa, K.S.; Mehane, S.A.; Soliman, K.S.; Diab, Z.E. Gravity profile interpretation using the R-parameter imaging technique with application to ore exploration. *Ore Geol. Rev.* **2020**, *126*, 103695. [[CrossRef](#)]
70. Santos, D.F.; Silva, J.B.C.; Lopes, J.F. In-depth 3D magnetic inversion of basement relief. *Geophysics* **2022**, *87*, 1–72. [[CrossRef](#)]
71. Mehane, S.A. Simultaneous Joint Inversion of Gravity and Self-Potential Data Measured Along Profile: Theory, Numerical Examples, and a Case Study from Mineral Exploration with Cross Validation From Electromagnetic Data. *IEEE Trans. Geosci. Remote Sens.* **2021**, *60*, 1–20. [[CrossRef](#)]
72. Won, I.J.; Bevis, M. Computing the gravitational and magnetic anomalies due to a polygon: Algorithms and Fortran subroutines. *Geophysics* **1987**, *52*, 232–238. [[CrossRef](#)]
73. Talwani, M.; Hertzler, J.R. Computation of magnetic anomalies caused by two dimensional bodies of arbitrary shape. *Geol. Sci.* **1964**, *9*, 464–480.
74. Talwani, M.; Worzel, J.L.; Landisman, M. Rapid gravity computations for two-dimensional bodies with application to the Mendocino submarine fracture zone. *J. Geophys. Res. Earth Surf.* **1959**, *64*, 49–59. [[CrossRef](#)]
75. Gunn, P. Regional magnetic and gravity responses of extensional sedimentary Basins. *AGSO J. Aust. Geol. Geophys.* **1997**, *17*, 115–131.
76. Benkhelil, M.G.; Ponsard, J.F.; Saugy, L. The Bornu-Benue Trough, the Niger Delta and its Offshore: Tectonosedimentary reconstruction during the cretaceous and tertiary from geophysical data and geology. In *Geology of Nigeria*; Kogbe, C.A., Ed.; Elizabethan Press: Lagos, Nigeria, 1975; pp. 277–309.
77. Ekwok, S.E.; Akpan, A.E.; Achadu, O.-I.M.; Thompson, C.E.; Eldosouky, A.M.; Abdelrahman, K.; Andráš, P. Towards Understanding the Source of Brine Mineralization in Southeast Nigeria: Evidence from High-Resolution Airborne Magnetic and Gravity Data. *Minerals* **2022**, *12*, 146. [[CrossRef](#)]
78. Ekwok, S.E.; Akpan, A.E.; Achadu, O.I.M.; Ulem, C.A. Implications of tectonic anomalies from potential field data in some parts of Southeast Nigeria. *Environ. Earth Sci.* **2022**, *81*, 6. [[CrossRef](#)]
79. Mineral Resources of the Western US. The Teacher-Friendly Guide to the Earth Scientist of the Western US. 2017. Available online: <http://geology.teacherfriendlyguide.org/index.php/mineral-w> (accessed on 9 January 2022).